Erik Hellström
Jacob Larimore
Anna Stefanopoulou

University of Michigan,
Ann Arbor, MI

Jeff Sterniak
Li Jiang

Robert Bosch LLC,
Farmington Hills, MI

Quantifying Cyclic Variability in a Multicylinder HCCI Engine With High Residuals

Cyclic variability (CV) in lean homogeneous charge compression ignition (HCCI) combustion at the limits of operation is a known phenomenon, and this work aims at investigating the dominant effects for the cycle evolution at these conditions in a multicylinder engine. Experiments are performed in a four-cylinder engine at the operating limits at late phasing of lean HCCI operation with negative valve overlap (nvo). A combustion analysis method that estimates the unburned fuel mass on a per-cycle basis is applied on both main combustion and the nvo period revealing and quantifying the dominant effects for the cycle evolution at high CV. The interpretation of the results and comparisons with data from a single-cylinder engine indicate that, at high CV, the evolution of combustion phasing is dominated by low-order deterministic couplings similar to the single-cylinder behavior. Variations, such as air flow and wall temperature, between cylinders strongly influence the level of CV but the evolution of the combustion phasing is governed by the interactions between engine cycles of the individual cylinders. [DOI: 10.1115/1.4007164]

1 Introduction

For favorable operating conditions, homogeneous charge compression ignition (HCCI) combustion is typically more fuel efficient while producing less emissions compared to spark-ignited or compression-ignited combustion. The operating range for HCCI is however limited and observed behavior indicates nonlinear feedback between engine cycles that can stabilize or destabilize the combustion process. Specifically, low cyclic variability (CV) is observed in the favorable range [1] while oscillations in combustion phasing with high CV at late phasing [2,3] and irregular phenomena at higher loads also have been reported [4].

HCCI is achieved in this work by a negative valve overlap (nvo) strategy where large amounts of the residual gases are trapped and recompressed through an early closing of the exhaust valve [5]. The focus here is on the CV exhibited in lean conditions at late phasing. High CV in HCCI with nvo at stoichiometric conditions with spark assist has been analyzed in [6,7] and shows qualitatively different dynamic behavior than the lean case. CV in HCCI achieved by heating the intake air is analyzed in [8] and the influence of different fuels is examined in [9,10]. Such strategies have a very low amount of residual gases compared to operating with nvo, which affects the feedback between cycles and modifies the combustion behavior. Stability analysis of HCCI with large amounts of residual gas is done in [11,12] where instabilities and sensitivity in phasing are attributed to the thermal dynamics. In [13] an extended two-state model is derived, including the fuel mass dynamics that predicts the observed behavior at high CV of lean HCCI in a single-cylinder engine.

Experiments and analysis with a recompression strategy at conditions with notable CV are reported in [14] for a single-cylinder engine and for multicylinder engines in [15,16]. These works examine the operating limits at different operating conditions and analyze relationships between successive cycles and [14,15] quantify these with linear correlation coefficients. Linear controllers for reducing CV are developed in [17] using variable valve timings and in [18] using fuel injection timing. The control is based on model linearization which captures the trend that one cycle with early combustion phasing is followed by a cycle with late phasing and vice versa. In [19] the trends in [14–18] are confirmed but it is also shown that, for higher CV, the cycle evolution is more complicated and is characterized by different patterns than treated in these works. Specifically, the relationship between cycles exhibits strong nonlinear behavior mainly due to the sharp falloff in the combustion efficiency for late phasing. The analysis method from [19] is improved here and applied on data from a four-cylinder engine. The results are interpreted and compared to data from the single-cylinder experiments in [19].

As a preliminary comparison, Fig. 1 shows return maps for combustion phasing and heat release from one cylinder in the four-cylinder engine and from the single cylinder. Return maps show the relationship between values of the variables in successive engine cycles and are a useful qualitative tool to study dynamic behavior. For example, return maps reveal nonlinear relationships that cannot be detected with linear correlation coefficients. Figure 1 shows that there are similarities in the dynamic behavior, especially for the phasing, despite the different engine platforms and operating conditions. Accordingly, the aim here is to quantify the coupling between engine cycles and the influence of variations between cylinders. To this end, the cycle evolution is investigated by analyzing thermodynamic variables and return maps. Symbolic time-series analysis is used to quantify the probabilities that certain sequences of cycles occur and enables a comparison between the four-cylinder engine and the single cylinder. It is thereby demonstrated that when CV increases, the evolution

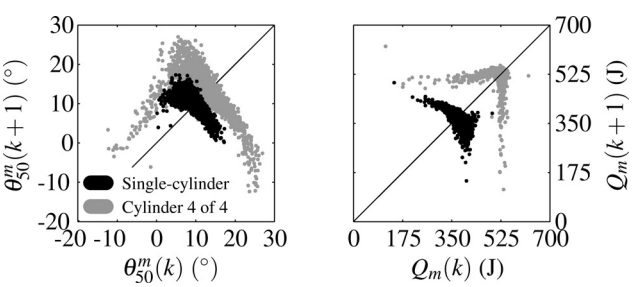

Fig. 1 Return maps for combustion phasing θ_{50}^m and gross heat release Q_m for a single-cylinder research engine (black) and for cylinder 4 of a four-cylinder engine (gray)

Contributed by the IC Engine Division of ASME for publication in the JOURNAL OF ENGINEERING FOR GAS TURBINES AND POWER. Manuscript received May 31, 2012; final manuscript received June 1, 2012; published online September 28, 2012. Editor: Dilip R. Ballal.

is dominated by the low-order deterministic coupling that is due to interactions between the engine cycles rather than between the cylinders in HCCI engines with recompression.

Coupling between cylinders in a four-cylinder HCCI engine controlled with exhaust throttles was analyzed in [20] through simulations and experiments. The coupling is found to be due to backflow in the intake manifold causing an increased pressure in the intake manifold. In contrast to these results, no communication was detected between cylinders that affected combustion phasing for a six-cylinder engine operating with nvo in [15]. Contributing factors to the different conclusions could be the different engine setups and that the effect observed in [20] was strongly affected by the intake valve timings. Our analysis show that the coupling between cycles is similar between the four-cylinder engine and the single cylinder while the large differences in the level of CV between cylinders are attributed to the high sensitivity at the edge of stable operation.

In the following two sections, the experimental conditions and the combustion analysis method are described. After that, the experimental results from the four-cylinder engine are interpreted and subsequently compared to data from a single-cylinder engine. The paper closes with the conclusions from the findings.

2 Experimental Method

Experiments were carried out in the Automotive Laboratory at the University of Michigan on a four-cylinder 2.0 L engine running on Tier-II certification fuel. The engine is a GM Ecotec modified for HCCI operation with increased compression ratio (to 11.25), modified camshaft (with lower lift and shorter duration), and a smaller turbocharger (a Borg-Warner KP31). The experiments were performed at constant speed of 2000 rpm and coolant temperature of 90 °C. The combustion limits were explored by varying nvo and studying the influence of the nvo on the CV. Nominal load was [4] bar net indicated mean effective pressure (IMEP). Fuel injection started at 60 deg after top dead center nvo (aTDCn). The chosen conditions were highly diluted and fairly lean with approximately 50% residual gas and a relative air-fuel ratio λ of 1.3–1.4. The focus here is on the combustion behavior without spark, however, spark ignition must be enabled to avoid fouling and is therefore set to 25 deg after top dead center main combustion (aTDCm) to ensure minimal influence on the combustion. Also, the influence of the spark is small during such diluted conditions. Cylinder pressure was sampled ten times per crank angle degree for 3000 engine cycles. The large number of cycles is necessary for observing the cycle dynamics in detail as noted in studies of high CV in lean SI and in stoichiometric HCCI [6,21].

3 Combustion Analysis

The analysis is based on standard methods for analysis of cylinder pressure combined with a method for estimating the unburned fuel on a per-cycle basis. This method was introduced in [19], and it is also shown here that the estimates converge independently of the guess for the unknown initial unburned mass. The estimation of the unburned fuel, which is the novel component in the combustion analysis, is described below, whereas a detailed description of the complete estimation routine, including charge mass estimation and heat release analysis, is found in [7,19]. The most important assumptions are that the gas flow through the engine is constant and that the heat transfer is described by the modified Woschni correlation from [22].

The engine cycle and important variables are defined in Fig. 2 for curves of pressure $p(\theta)$ and accumulated heat release $Q(\theta)$. Note that the heat release analysis is applied on both the main combustion event, between intake valve closing (ivc) and exhaust valve opening (evo), and the nvo period, between exhaust valve closing (evc) and intake valve opening (ivo). The top dead center of the main combustion is defined as 0 deg and a cycle is defined to start at ivc. The total heat release in cycle k during main

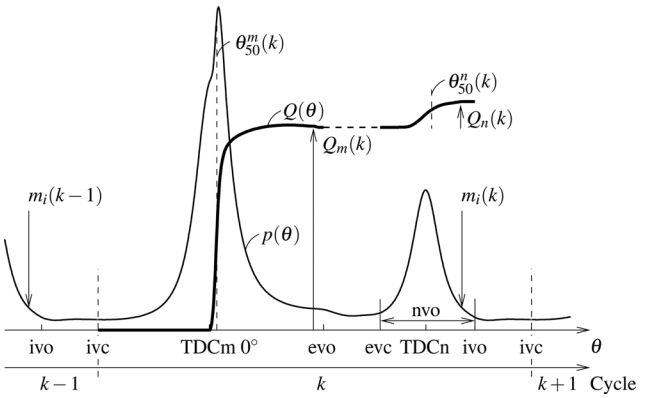

Fig. 2 Definition of the engine cycle and important variables for curves of pressure $p(\theta)$ (thin line) and heat release $Q(\theta)$ (thick line)

combustion and the nvo period are denoted by $Q_m(k)$ and $Q_n(k)$, and the 50% burn angles are denoted by $\theta_{50}^{m}(k)$ and $\theta_{50}^{n}(k)$, respectively.

The analysis routine is iterated until the combustion efficiencies, defined later in Eq. (8), converge at which point the governing relations of mass and energy conservation are satisfied. Although it is shown that the choice of initial values is not critical, a good initial guess, e.g., based on the average exhaust composition, may reduce the required number of iterations. Here the values for complete combustion are employed. The main outputs from the routine are the thermodynamic state, pressure and temperature, and cycle-resolved values of unburned fuel and combustion efficiencies.

3.1 Unburned Fuel. The unburned fuel mass in each engine cycle is estimated based on a difference equation for mass conservation that represents the evolution of the unburned mass. The inputs are injected fuel mass, heat release values, and residual gas fraction which are known from the other steps in the estimation routine [19]. The estimation requires an initial guess but it is shown below that the method converges independently of the value of the initial guess. The estimate is subsequently used to obtain estimates of combustion efficiencies on a per-cycle basis. The algorithm and its convergence are discussed below.

The fuel mass $m_f(k)$ in the beginning of cycle k (at ivc) is

$$m_f(k) = m_i(k-1) + m_u(k) \tag{1}$$

where $m_i(k-1)$ is the fuel mass injected in the nvo period of the previous cycle and $m_u(k)$ is the unburned fuel mass, in this cycle, carried over from previous cycles. A fraction $\eta_m(k)$ of $m_f(k)$ is consumed during the main combustion and, at evc, a fraction $x_r(k)$ of the residual gases is trapped. Of the remaining fuel mass, a fraction $\eta_n(k)$ is consumed during the nvo period. The unburned fuel mass carried over to the next cycle $k+1$ is then

$$m_u(k+1) = x_r(k)[1-\eta_m(k)][1-\eta_n(k)]m_f(k) \tag{2}$$

based on the assumption that the residuals are homogeneously mixed. The combustion efficiencies in Eq. (2) are unknown but can be related to the total heat release. The gross heat released during the main combustion Q_m is calculated using cylinder pressure data [19] and is related to the fuel mass and efficiency η_m as

$$m_f(k)\eta_m(k) = \frac{Q_m(k)}{q_{\text{lhv}}} \tag{3}$$

where q_{lhv} is the lower heating value for the fuel. Similarly, the gross heat released during the nvo period Q_n is used to obtain

$$m_f(k)\eta_n(k) = \frac{Q_n(k)}{[1-\eta_m(k)]x_r(k)q_{\text{lhv}}} \tag{4}$$

Note that Eqs. (3) and (4) are based on assuming that the energy release is proportional to the mass of fuel consumed and that any incomplete intermediate combustion reactions will be aliased into the mass estimates. Combining Eqs. (1)–(4) yields the final equation for predicting the unburned fuel mass:

$$m_u(k+1) = x_r(k)\left[m_i(k-1) + m_u(k) - \frac{Q_m(k)}{q_{\text{lhv}}}\right] - \frac{Q_n(k)}{q_{\text{lhv}}} \tag{5}$$

The inputs to this model are injected fuel m_i together with the total gross heat releases (Q_m, Q_n) and residual gas fraction x_r that are calculated according to [7,19]. The fuel injection is constant here, $m_i(k) = \bar{m}_i$, since constant fueling was used in the experiments. Given these inputs, Eq. (5) is iterated given an initial condition $m_u(0)$. This value is unknown but, as shown below, it turns out to be of little significance since its influence quickly vanishes.

3.1.1 Convergence. Equation (5) can be compactly written as

$$m_u(k+1) = x_r(k)m_u(k) + a(k) \tag{6}$$

where the coefficient $x_r(k)$ and the forcing term $a(k)$,

$$a(k) = x_r(k)\left[\bar{m}_i - \frac{Q_m(k)}{q_{\text{lhv}}}\right] - \frac{Q_n(k)}{q_{\text{lhv}}}$$

are known and vary with cycle. The general solution to the difference equation (6) for $k = 1, 2, \ldots$ is

$$m_u(k) = a(k-1) + \sum_{i=0}^{k-2} a(i) \prod_{j=i+1}^{k-1} x_r(j) + m_u(0) \prod_{i=0}^{k-1} x_r(i) \tag{7}$$

Since $0 < x_r(k) < 1$ holds in practice, the term with $m_u(0)$ eventually vanishes and it can be concluded that the series (5) is convergent. The unknown initial condition $m_u(0)$ can thus be guessed since, whatever the guess, its influence will vanish and the result will be unique after a transient. Moreover, it is seen from Eq. (7) that the convergence rate depends only on the value of $x_r(k)$. For the influence of the initial condition to be reduced to 10^{-m}, $n = \lceil -m \log_{10}^{-1} x_r \rceil$ iterations are required.

3.1.2 Combustion Efficiencies. When the unburned fuel mass is computed, Eqs. (3) and (4) give

$$\eta_m(k) = \frac{Q_m(k)/q_{\text{lhv}}}{m_f(k)}, \quad \eta_n(k) = \frac{Q_n(k)/q_{\text{lhv}}}{x_r(k)\left[m_f(k) - \dfrac{Q_m(k)}{q_{\text{lhv}}}\right]} \tag{8}$$

as approximations for the efficiencies. Due to the unknown initial condition $m_u(0)$, these are valid for $k \gtrapprox 12$. The influence of the unknown $m_u(0)$ is considered negligible when its influence on $m_u(k)$ is reduced by $1/1000$. In this work the value of x_r is not higher than 54% and, from the discussion in the previous paragraph, 12 cycles are thus sufficient. The convergence is illustrated in Fig. 3, on experimental data for a condition with high CV for initial conditions $m_u(0)$ ranging from 0% to 100% of $\bar{m}_i$. Based on these results, an initial guess of $m_u(0) = 0$ is applied and the first 12 cycles (of the 3000 cycles of data) are discarded in the analysis.

4 Results

This thermodynamic analysis is applied to several operating conditions at the boundary of stable combustion at late combustion phasing. Two representative operating conditions with different nvo are selected and reported here. The measured and estimated quantities are first examined revealing and quantifying the dominant coupling and cause for the behavior at conditions with high CV. Additionally, the cycle evolution is analyzed using return maps and symbol statistics. These mathematical tools provide a systematic method to discover dynamic interactions and reveal unstable behavior in phasing and heat release.

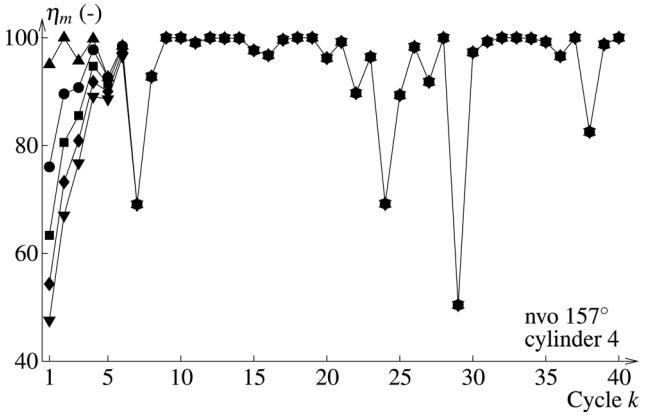

Fig. 3 Estimates of the efficiency η_m for 40 cycles from cylinder 4. The symbols (▲, ●, ■, ◆, ▼) represents initial conditions $m_u(0)$ equal to (0, 25, 50, 75, 100)% of the injected fuel mass $\bar{m}_i$.

Table 1 The residual gas fraction (x_r), combustion phasing (θ_{50}^m), standard deviation of θ_{50}^m ($\sigma_{\theta_{50}^m}$), and coefficient of variation of IMEP (CoV_{IMEP}) for two selected operating conditions

nvo	160 deg				157 deg			
Cylinder	1	2	3	4	1	2	3	4
x_r (%)	55	55	53	53	53	53	50	51
θ_{50}^m (deg)	7.6	8.6	7.1	9.0	11.0	12.1	11.8	12.5
$\sigma_{\theta_{50}^m}$ (deg)	1.2	1.2	1.3	1.4	1.9	4.0	3.3	4.9
CoV_{IMEP} (%)	1.5	1.5	1.3	1.4	2.4	9.0	6.7	7.9

The first operating condition has an nvo of 160 deg and acceptable CV while the second condition has an nvo of 157 deg and high CV. The nominal experimental conditions are given above while Table 1 shows a number of variables that describe the change when reducing the nvo while keeping other actuators constant. With the smaller nvo the residual gas fraction decreases 2%–3% for all cylinders and λ, measured with one sensor in the exhaust, increases from 1.3 to 1.4. The phasing θ_{50}^m retards 3.4 deg–3.5 deg, except for cylinder 3 that retards 4.7 deg from TDCm. The standard deviation $\sigma_{\theta_{50}^m}$ and the coefficient of variation of IMEP CoV_{IMEP} increase notably. The largest increases are seen for cylinders 2 and 4.

4.1 Thermodynamic Phenomena. From the measured cylinder pressure and estimated temperature for the two cases shown in Fig. 4, it is seen that reducing the nvo increases the CV for all cylinders.

The increased variability can be seen in the spread of the observed peak pressures and pressure rise rates during main combustion. In the nvo period for the high CV case, the estimated temperatures are similar or higher than the case with low CV and sometimes reach values similar to those during main combustion. Furthermore, the highest peak cylinder pressures, during main combustion and the nvo period, are observed for the case with high CV. These observations suggest that there is unburned fuel that produces heat release during recompression and also that unburned fuel may carry over and release heat in the next main combustion event. The level of CV differs between the cylinders,

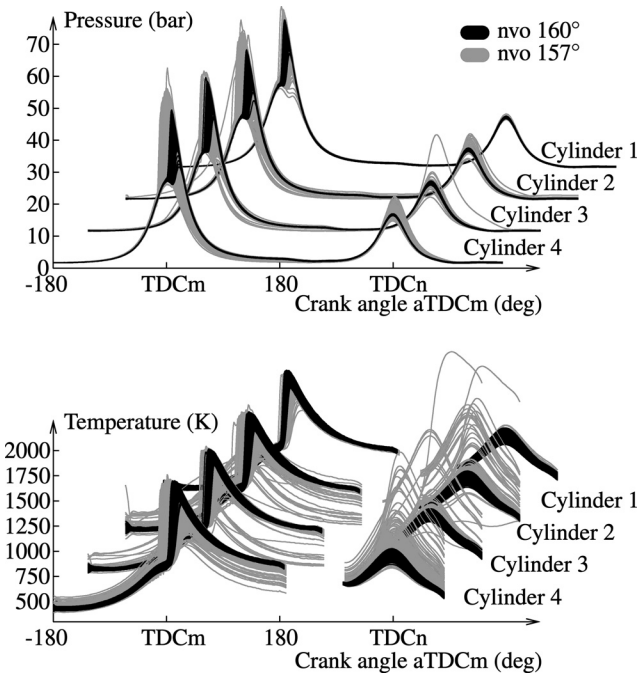

Fig. 4 Pressure and temperature for low and high CV

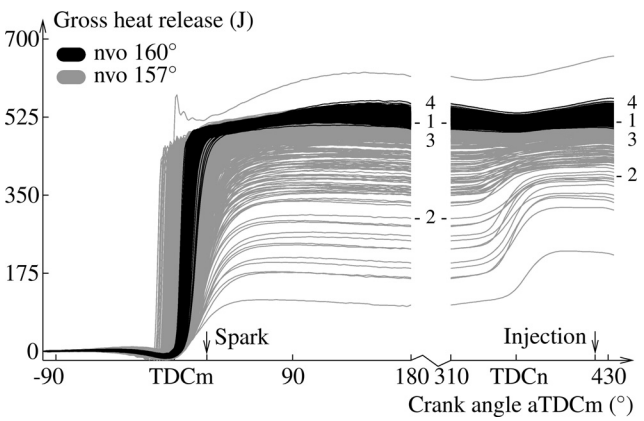

Fig. 5 Gross heat release in cylinder 4 for low and high CV. Four consecutive cycles are numbered where all except the second cycle have similar total heat release. These cycles are also shown in Figs. 6–9.

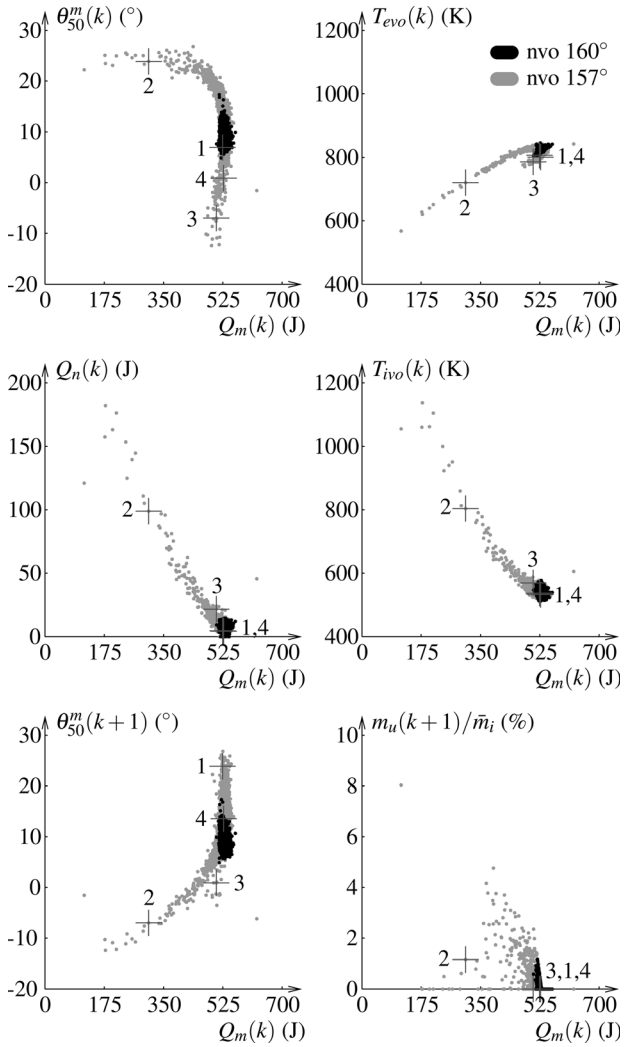

Fig. 6 Cylinder 4 heat release during the main combustion $Q_m(k)$ versus main combustion phasing $\theta_{50}^m(k)$, temperature at evo $T_{evo}(k)$, heat release during the nvo period $Q_n(k)$, temperature at ivo $T_{ivo}(k)$, combustion phasing $\theta_{50}^m(k+1)$, and unburned fuel $m_u(k+1)$

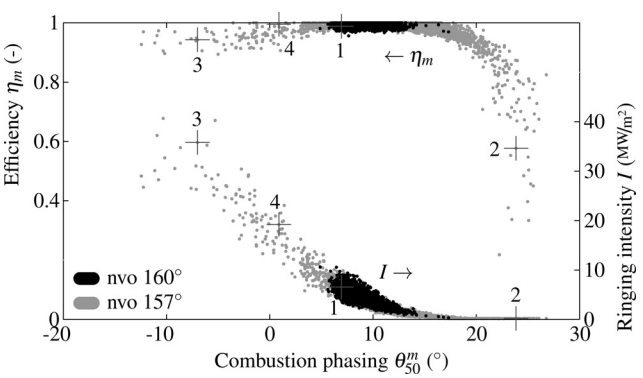

Fig. 7 Combustion efficiency η_m and ringing intensity I versus phasing for low and high CV showing the increased spread of values for high CV. The numbered cycles are also shown in Figs. 5, 6, 8, and 9.

as seen in Fig. 4 and Table 1 where cylinder 1 has earlier phasing and much lower CV than the other three. To study the effects of CV in detail, the fourth cylinder, with highest $\sigma_{\theta_{50}^m}$, is studied in Figs. 5–7.

The gross heat release for cylinder 4 is shown in Fig. 5 for the two operating conditions. A coupling and complementarity of the heat release in the main combustion and the recompression appears in our data. Cycles with a low accumulated heat release during main combustion are followed by a noticeable heat release during recompression with a relatively slow burn rate. This is exemplified by the sequence of consecutive cycles marked in Fig. 5. The start of injection is late in the nvo period (60 deg aTDCn) and does not have any appreciable influence on the heat release, which justifies the use of Eq. (4). To clarify the cyclic coupling, Fig. 6 shows a number of variables versus the heat release during main combustion $Q_m(k)$ in cycle k for cylinder 4 in the two operating conditions with different nvo. The top two rows show the main combustion phasing $\theta_{50}^m(k)$, temperature at evo $T_{\text{evo}}(k)$, heat release during the nvo period $Q_n(k)$, and temperature at ivo $T_{\text{ivo}}(k)$ versus $Q_m(k)$ in the same cycle k. The bottom row shows the phasing of the next cycle $\theta_{50}^m(k+1)$, and the unburned fuel that is carried over to the next cycle $m_u(k+1)$ versus $Q_m(k)$. When nvo decreases, CV increases, and trends appear

of which the most evident are now summarized. Late phasing $\theta_{50}^m(k)$ in cycle k is associated with a low heat release $Q_m(k)$ which in turn leads to a decreased $T_{\text{evo}}(k)$. This decrease is, however, canceled by the nvo heat release so that $T_{\text{ivo}}(k)$ increases which advances the phasing $\theta_{50}^m(k+1)$ of the next cycle $k+1$. Also, even if there is heat release during nvo, some of the unburned fuel, up to 8% as estimated by Eq. (5), carries over to the next cycle. The complementarity of the heat release in the main combustion and the nvo period has been observed earlier in experiments [14,16] and predicted in simulations [23]. However, the estimates of the unburned fuel mass suggest that not all of the remaining fuel is necessarily consumed during nvo and a fraction of it may carry over to the next cycle. An example of these trends is the sequence of four cycles marked in Figs. 5 and 6.

Figure 7 shows the main combustion efficiency η_m and the ringing intensity I versus the main combustion phasing θ_{50}^m. The efficiency η_m is computed from Eq. (8) and the intensity I is computed according to the correlation developed by Eng [24, Eq. (16)]. The average I for all cycles is 4.5 and 2.8 MW/m^2 for the low and high CV case, respectively. Although the average is lower, the spread of I in an individual cycle is much larger than that for the low CV. The efficiency η_m decreases with later phasing, whereas the intensity I increases with early phasing, as expected. These early cycles have high I due to large pressure oscillations that may increase the heat transfer. This effect is not captured in the heat transfer model, which is the modified Woschni from [22]. An underestimated heat transfer will lead to a lower estimated value of η_m, see Eq. (8), and this is suspected to be a contributing factor to the drop in η_m for early phasing. The sharp drop in efficiency at very late phasing shows that the sensitivity with respect to phasing increases dramatically. Thus, the efficiency curve, which determines the unburned fuel mass after main combustion, is an important nonlinear relation for accurately describing the coupling between cycles. The importance is further illustrated in the following analysis using return maps.

4.2 Return Maps. The causality of important variables and the influence of Q_m were shown in Fig. 6. Another useful graphical tool for studying the cycle evolution of variables are return maps, which show the relationship between subsequent values of a variable. Most importantly, return maps reveal low-order deterministic features even when these are nonlinear.

A return map or lag-1 map, shown in Figs. 8 and 9, is a plot of a variable $x(k)$ at cycle k versus the value at the next cycle $x(k+1)$. Figure 8 shows the return maps for combustion phasing θ_{50}^m for the two operating conditions studied. For nvo = 160 deg, the return maps show clouds without clear structure. With nvo = 157 deg, the CV increases and characteristic patterns emerge. The patterns are more pronounced for the cylinders with higher CV but all share the same features. The main characteristics of the patterns can be described by a cluster of cycles stretching out perpendicular to the diagonal and another part bending the left tip and extending down to the left. The perpendicular part indicates an unstable behavior where θ_{50}^m alternates between early and late phasing. The oscillations in θ_{50}^m can have a large amplitude as shown by the magnitude of the perpendicular cluster of cycles which is most pronounced in cylinder 4. The right part of the cluster together with the bent part show that there is a limit for the amplitude value so that when the amplitude is sufficiently large the combustion does, at least temporarily, recover to a phasing closer to the average. The sequence discussed earlier for cylinder 4 in the high CV case is marked in Fig. 8 and is an illustration of a large amplitude oscillation followed by a recovery. The overall patterns for θ_{50}^m for high CV show a clear asymmetry about the diagonal. An asymmetric pattern implies an asymmetry in time which means that the evolution of θ_{50}^m is due to nonlinear dynamics or non-Gaussian noise, or both [25].

The patterns for the heat release Q_m, shown in Fig. 9, are characterized by two parts, one stretching out vertically and another

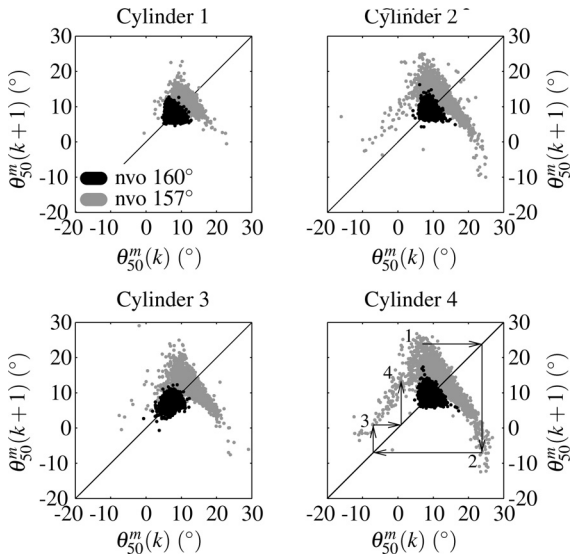

Fig. 8 Return maps for phasing θ_{50}^m. The marked sequence for cylinder 4 corresponds to the numbered cycles in Figs. 5–7, and 9.

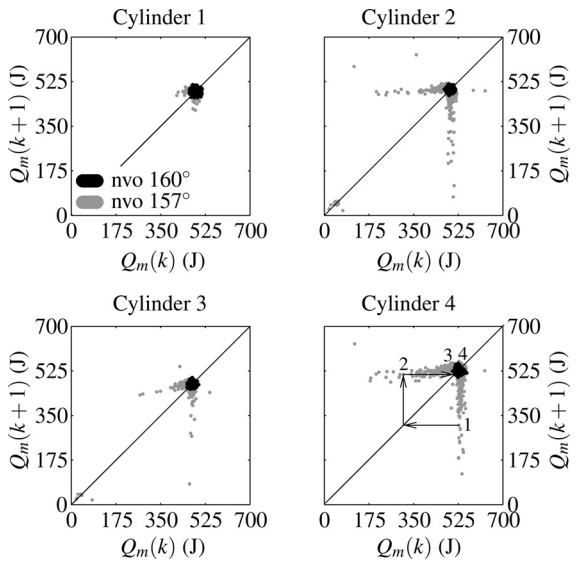

Fig. 9 Return maps for total heat release Q_m. The marked sequence for cylinder 4 corresponds to the numbered cycles in Figs. 5–8.

extending to the left. An unstable behavior is also seen here in the vertical part indicating that a cycle with an average heat release can be followed by a cycle with a large range of values. This is related to the fact that the efficiency and, thus, Q_m have a very steep falloff for late phasing, as demonstrated in Figs. 6 and 7. A late cycle with low heat release is, in turn, followed by a cycle with approximately average heat release as indicated by the left part of the pattern that stretches out almost horizontally. The sequence marked for cylinder 4 in Figs. 7–9 illustrates these trends.

The characteristics for the evolution of the combustion phasing show that large excursions are preceded by an unstable oscillation with large amplitudes. On the other hand, the heat release showed an unstable behavior where there could be a large change from one cycle to the next which is a result of the nonlinear efficiency curve, see Fig. 7 where it is shown that the phasing may vary in a fairly large range with similar efficiency but drop off sharply when the phasing passes a threshold.

4.3 Symbol Statistics. Symbolic time-series analysis is a technique for analyzing noisy data especially for nonlinear and possibly chaotic systems, see [26] for a presentation of the technique for studying combustion data. The return maps give important insights into the dynamic behavior between successive cycles and primarily in a qualitative manner while symbolic time-series analysis is a method to study sequences of several cycles and also to quantify the probability for certain sequences to occur. This quantification enables the comparison of the most probable sequences observed among different cylinders and engines. In particular, the symbol statistics allow us to compare the high CV behavior at late phasing in the multicylinder engine with the single cylinder.

To obtain the symbol statistics, the measurement values, e.g., θ_{50}^m, are first partitioned into a set of n discrete symbols and then the statistics for the occurrence of symbol sequences $s = s_1 s_2 \cdots s_L$ of length L are computed. The partitioning is done so that every symbol is equally probable. The relative frequency for any order of cycles is then n^{-L} if the evolution is purely random. In other words, the values of combustion phasing θ_{50}^m and heat release Q_m are categorized into n bins and the boundaries of the bins are chosen so that the number of samples are the same in each bin.

The number of categories, the symbol-set size n, is chosen so as to discriminate data points that have extreme values from the ones close to the median or the ones with intermediate values. The symbol-set size n is chosen to be 5, which gives reasonable granularity for phasing and heat release. Consequently, this choice distinguishes between very early, early, median, late, and very late values of the combustion phasing. For the heat release, the categories are very low, low, median, high, and very high values. For a compact representation, these categories are labeled with a number from 0 to 4. As an example, the partitioning for cylinder 4 in the high CV case is shown in Table 2. The intervals for the very early and very late categories are wider than the others due to the equiprobable partitioning and the fact that there are more data points close to the median than farther away. Note that the partitioning is different for each data set, meaning that each cylinder in the respective case has its own partitioning due to the equiprobable requirement.

The symbol-sequence length L is chosen to be 3 by using the approach in [26] utilizing a modified Shannon entropy. Roughly speaking, the aim is to choose L so as to best identify the deterministic features in the data. Using the labeling of the categories with a number from 0 to $n-1=4$, the cycle evolution is compactly described by sequences of $L=3$ of these numbers. To illustrate, consider the sequences (140,403) for the phasing θ_{50}^m. These represent sequences of cycles $s = s_1 s_2 s_3$, where the values of θ_{50}^m are categorized as shown in Table 3.

The symbol statistics for the combustion phasing θ_{50}^m and for the heat release Q_m are shown in Figs. 10 and 11, where the four sequences with highest probability are marked in the figure. Note that a sequence is a number in the base $n=5$ while the abscissa in Figs. 10 and 11 is, for convenience, in base 10. For example the sequence 140 in base 5 is 45 in base 10.

Figure 10 shows that, when reducing the nvo, sequences appear that have probabilities clearly higher than $n^{-L} = 0.8\%$ (shown with the dashed line) for a random evolution and this is most evident for cylinders 2 and 4 that have the highest CV, see Table 1. The two most common sequences of θ_{50}^m for all cylinders that emerge at high CV are 040 and 404, representing oscillations between the extreme values of the partitioning. The sequence 140 is the third most common and is a sequence with increasing amplitude, see Table 3. These sequences correspond to the qualitative features discussed above for the return maps of unstable oscillations. Note that it also can be concluded that common sequences are combinations such as 0404, 4040, and 1404. For example,

Table 2 The partitioning of the combustion phasing data, from cylinder 4 in the case with high CV, such that each symbol is equally probable

Symbol	Definition
(0) very early	$-12 < \theta_{50}^m < 10$
(1) early	$10 < \theta_{50}^m < 12$
(2) median	$12 < \theta_{50}^m < 14$
(3) late	$14 < \theta_{50}^m < 16$
(4) very late	$16 < \theta_{50}^m < 27$

Table 3 Examples of symbol sequences

Sequence	Description
$s = 140$	An early cycle (1) is followed by a very late cycle (4) which is followed by a very early cycle (0).
$s = 403$	A very late cycle (4) is followed by a very early cycle (0) which is followed by a late cycle (3).

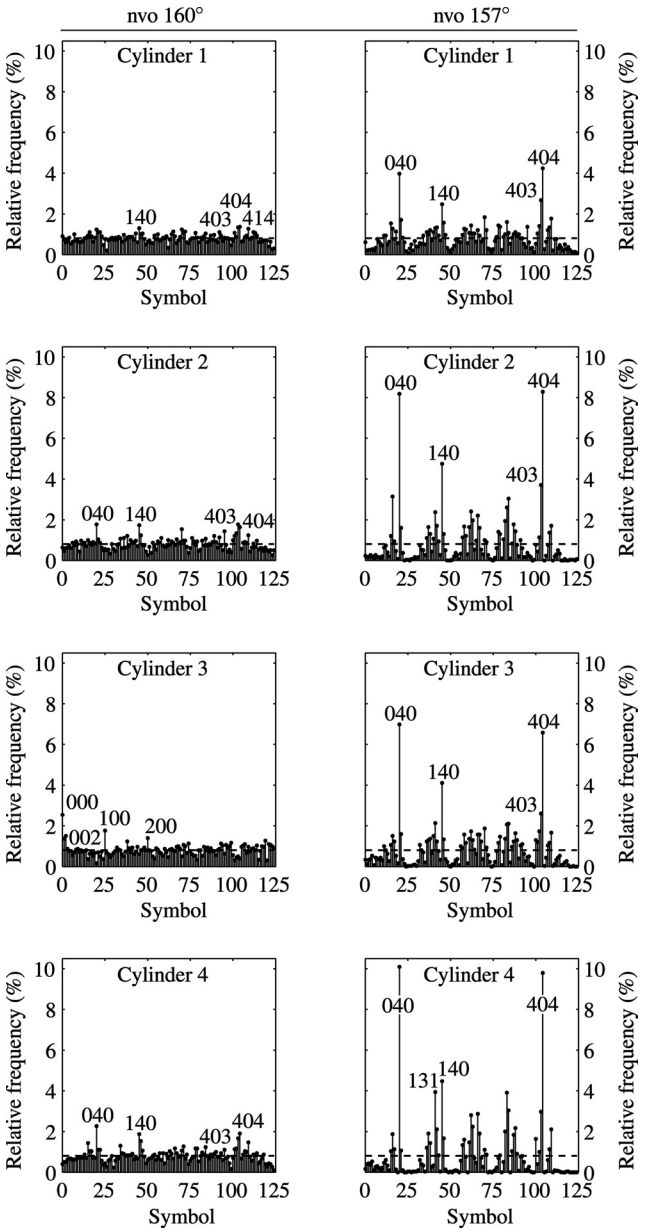

Fig. 10 Symbol statistics for combustion phasing θ_{50}^m

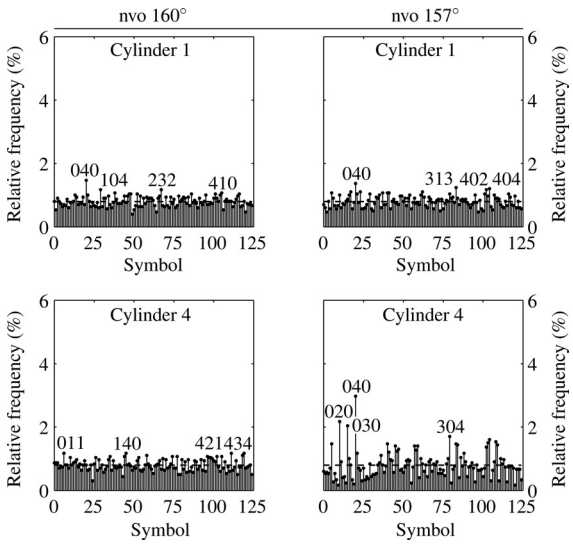

Fig. 11 Symbol statistics for the gross heat release Q_m

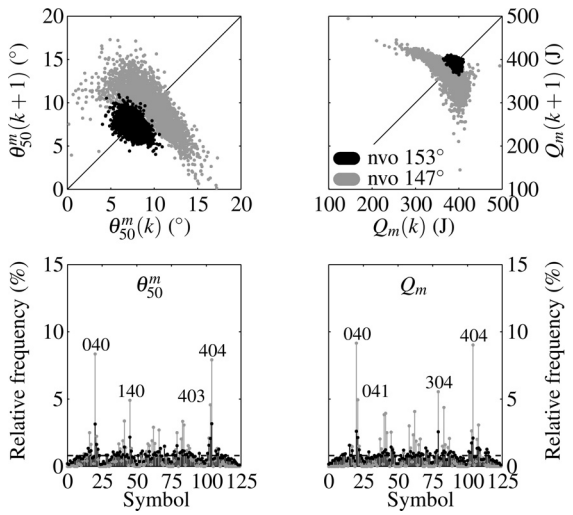

Fig. 12 Return maps and symbol statistics for single-cylinder experiments reported in [19]

after 040 one of the sequences (400,401,402,403,404) must follow of which 404 has the highest probability. The fourth most common sequence is 403 for cylinders 1 through 3 and common combinations are thus also 0403 and 1403. In contrast to 140, 403 is a sequence with decreasing amplitude, see Table 3. For cylinder 4, with the highest CV, the probability of 403 sequences are diminished and 131, an oscillation where the amplitude is approximately sustained, is instead the fourth most common sequences of cycles. Note that for cylinders 2 and 4 the sequences that are more pronounced for higher CV, i.e., with nvo of 157 deg, already can be distinguished for lower CV, i.e. with nvo of 160 deg. This cannot be easily determined by looking at the return maps in Fig. 8 or the measures $\sigma_{\theta_{50}^m}$ and $\mathrm{CoV}_{\mathrm{IMEP}}$ in Table 1. The asymmetry found in the return maps can also be seen in the symbol statistics by frequency mismatches between time inverses of sequences [26], here exhibited by the sequences 140 and 403.

The statistics for the gross heat release Q_m are shown in Fig. 11, cylinders 1 and 4 are shown to conserve space. Distinctive sequences appear in cylinder 4 where oscillating sequences emerge with approximately sustained amplitude (020,040,030) and with increasing amplitude (304). The most common sequences for cylinders 2 and 3, which are not shown, are (030,040,304,404) and (020,040, 041,404), respectively, which show the same characteristics with the exception of the sequence with reduced amplitude (041) for cylinder 3.

5 Comparison With Single-Cylinder Data

The cycle evolution is here investigated in experimental data [19] from a single-cylinder research engine and compared with the multicylinder data qualitatively using return maps and quantitatively using symbol statistics. The single-cylinder experiments were performed on an engine with a compression ratio of 12.4 running on research grade gasoline. The nominal operating conditions were $\lambda = 1.7$, net IMEP of 2.8 bars, and 2000 rpm. Despite the different engine platforms and conditions, the dynamic behavior for high CV shows strong similarities suggesting that the governing coupling is between cycles of the individual cylinders.

It should be noted that the estimated combustion phasing is not as sensitive as the value of the gross heat release to the errors in the estimated heat transfer that were discussed in connection with the efficiency estimates. Also, the estimated phasing is robust against noise due to the fast nature of HCCI combustion [27]. For these reasons, stronger emphasis is put on the comparison of the combustion phasing evolution than the heat release evolution.

Figure 12 shows the return maps and symbol statistics for phasing θ_{50}^m and heat release Q_m for two settings of nvo transitioning from low to high CV. The symbol-set size n is 5 and sequence length L is 3 as used above. Comparison of the return maps in Fig. 12 with Figs. 8 and 9 shows that there are clear geometric similarities. In particular, the θ_{50}^m patterns are very similar and are described by one part perpendicular to the diagonal, indicating unstable oscillations, and a bent tip, showing a recovery behavior. This is confirmed and quantified by the symbol statistics that show similar frequency distribution and also good agreement for the dominating sequences. The return maps for the heat release show an unstable vertical direction in both cases but the part extending to the left shows different behavior. For the four-cylinder case, in Fig. 9, a cycle with low heat release, far down the vertical part, is followed by a heat release with a value close to but lower than the average. The single-cylinder data shown in the top right plot in Fig. 12, conversely to the four-cylinder engine data, show that a cycle with low heat release is followed by a heat release higher than average. Comparing the symbol statistics for the heat release from the single-cylinder and from the four-cylinder engine show that the agreement is not as good as for the phasing.

6 Conclusions

High CV conditions in a four-cylinder engine operating HCCI by negative valve overlap is analyzed and compared to single-cylinder data. The key findings are:

- The dominating effects for high CV are recycled thermal energy and recycled unburned fuel in the residual gases.
- As the combustion phasing retards and the CV increases, the cycle evolution is governed by these low-order deterministic mechanisms rather than random or high-order dynamic behavior.
- Due to the high sensitivity of the conditions at the edge of steady operation, small variations between cylinders are amplified at high CV conditions and the variations between cylinders are higher than at low CV.
- The in-cylinder dynamics of the combustion phasing are dominated by the coupling between cycles, while the variations between cylinders, for example, due to flow phenomena and different wall temperatures, strongly influence the level of CV.

These findings collectively show that each cylinder can be viewed as a separate feedback control loop and that the low-order model developed in [13], which predicted the behavior of the combustion phasing for a single-cylinder engine, can be used to capture the behavior in a multicylinder engine with the proper model inputs for each cylinder.

Acknowledgment

We thank S. Bohac and A. Vaughan at the University of Michigan for setting up and maintaining the engine test cell. This work is supported by the Department of Energy (National Energy Technology Laboratory) under award number DE-EE0003533 and performed as a part of the ACCESS project consortium (Robert Bosch LLC, AVL Inc., Emitec Inc.) under the direction of Principal Investigator H. Yilmaz, Robert Bosch, LLC.

Nomenclature

m_f = total in-cylinder fuel mass
m_i = injected fuel mass
m_u = unburned fuel mass
ivo/c = intake valve opening/closing
evo/c = exhaust valve opening/closing
nvo = negative valve overlap (evc–ivo)
m, n = sub/superscripts denoting the main combustion period (ivc–evo) and the nvo period (evc–ivo)
$\theta_{50}^m, \theta_{50}^n$ = combustion phasing for main/nvo period
Q_m, Q_n = gross heat release for main/nvo period
η_m, η_n = combustion efficiency for main/nvo period

References

[1] Law, D., Kemp, D., Allen, J., Kirkpatrick, G., and Copland, T., 2001, "Controlled Combustion in an IC-Engine With a Fully Variable Valve Train," SAE Technical Paper No. 2001-01-0251.
[2] Thring, R. H., 1989, "Homogeneous-Charge Compression-Ignition (HCCI) Engines," SAE Technical Paper No. 892068.
[3] Koopmans, L., and Denbratt, I., 2001, "A Four Stroke Camless Engine, Operated in Homogeneous Charge Compression Ignition Mode With Commercial Gasoline," SAE Technical Paper No. 2001-01-3610.
[4] Olsson, J.-O., Tunestål, P., Johansson, B., Fiveland, S., Agama, R., Willi, M., and Assanis, D., 2002, "Compression Ratio Influence on Maximum Load of a Natural Gas Fueled HCCI Engine," SAE Technical Paper No. 2002-01-0111.
[5] Willand, J., Nieberding, R.-G., Vent, G., and Enderle, C., 1998, "The Knocking Syndrome—Its Cure and Its Potential," SAE Technical Paper No. 982483.
[6] Wagner, R. M., Edwards, K. D., Daw, C. S., Green, J. B., Jr., and Bunting, B. G., 2006, "On the Nature of Cyclic Dispersion in Spark Assisted HCCI Combustion," SAE Technical Paper No. 2006-01-0418.
[7] Larimore, J., Hellström, E., Sterniak, J., Jiang, L., and Stefanopoulou, A. G., 2012, "Experiments and Analysis of High Cyclic Variability at the Operational Limits of Spark-Assisted HCCI Combustion," Proc. American Control Conference, pp. 2072–2077.
[8] Ghazimirsaied, A., Shahbakhti, M., and Koch, C. R., 2010, "HCCI Engine Combustion Phasing Prediction Using a Symbolic-Statistics Approach," ASME J. Eng. Gas Turbines Power, **132**(8), p. 082805.
[9] Sjöberg, M., and Dec, J. E., 2007, "Comparing Late-Cycle Autoignition Stability for Single- and Two-Stage Ignition Fuels in HCCI Engines," Proc. Combust. Inst., **31**(2), pp. 2895–2902.
[10] Shahbakhti, M., and Koch, C. R., 2008, "Characterizing the Cyclic Variability of Ignition Timing in a Homogeneous Charge Compression Ignition Engine Fuelled With n-Heptane/Iso-Octane Blend Fuels," Int. J. Engine Res., **9**(5), pp. 361–397.
[11] Chiang, C., and Stefanopoulou, A. G., 2007, "Stability Analysis in Homogeneous Charge Compression Ignition (HCCI) Engines With High Dilution," IEEE Trans. Control Syst. Technol., **15**(2), pp. 209–219.
[12] Kang, J.-M., 2010, "Sensitivity Analysis of Auto-Ignited Combustion in HCCI Engines," SAE Technical Paper No. 2010-01-0573.
[13] Hellström, E., and Stefanopoulou, A. G., 2011, "Modeling Cyclic Dispersion in Autoignition Combustion," Proc. 50th IEEE Conference on Decision and Control, pp. 6834–6839.
[14] Koopmans, L., Backlund, O., and Denbratt, I., 2002, "Cycle to Cycle Variations: Their Influence on Cycle Resolved Gas Temperature and Unburned Hydrocarbons From a Camless Gasoline Compression Ignition Engine," SAE Technical Paper No. 2002-01-0110.
[15] Persson, H., Pfeiffer, R., Hultqvist, A., Johansson, B., and Ström, H., 2005, "Cylinder-to-Cylinder and Cycle-to-Cycle Variations at HCCI Operation With Trapped Residuals," SAE Technical Paper No. 2005-01-0130.
[16] Karagiorgis, S., Collings, N., Glover, K., Coghlan, N., and Petridis, A., 2006, "Residual Gas Fraction Measurement and Estimation on a Homogeneous Charge Compression Ignition Engine Utilizing the Negative Valve Overlap Strategy," SAE Technical Paper No. 2006-01-3276.
[17] Jungkunz, A. F., Liao, H.-H., Ravi, N., and Gerdes, J. C., 2010, "Reducing Combustion Variation of Late-Phasing HCCI With Cycle-to-Cycle Exhaust Valve Timing Control," IFAC Symp. on Advances in Automotive Control.
[18] Jungkunz, A. F., Liao, H.-H., Ravi, N., and Gerdes, J. C., 2011, "Combustion Phasing Variation Reduction for Late-Phasing HCCI Through Cycle-to-Cycle Pilot Injection Timing Control," ASME Paper No. DSCC2011-6091.
[19] Hellström, E., Stefanopoulou, A. G., Vávra, J., Babajimopoulos, A., Assanis, D., Jiang, L., and Yilmaz, H., 2012, "Understanding the Dynamic Evolution of Cyclic Variability at the Operating Limits of HCCI Engines With Negative Valve Overlap," SAE Int. J. Engines, **5**(3), pp. 995–1008, Technical Paper No. 2012-01-1106.
[20] Souder, J. S., Mehresh, P., Hedrick, J. K., and Dibble, R. W., 2004, "A Multi-Cylinder HCCI Engine Model For Control," ASME Paper No. IMECE2004-61966.
[21] Daw, C., Kennel, M., Finney, C., and Connolly, F., 1998, "Observing and Modeling Nonlinear Dynamics in an Internal Combustion Engine," Phys. Rev. E, **57**(3), pp. 2811–2819.
[22] Chang, J., Güralp, O., Filipi, Z., Assanis, D., Kuo, T.-W., Najt, P., and Rask, R., 2004, "New Heat Transfer Correlation for an HCCI Engine Derived From Measurements of Instantaneous Surface Heat Flux," SAE Technical Paper No. 2004-01-2996.
[23] Knierim, K. L., Park, S., Ahmed, J., Kojic, A., Orlandini, I., and Kulzer, A., 2008, "Simulation of Misfire and Strategies for Misfire Recovery of Gasoline HCCI," Proc. American Control Conference, pp. 3947–3952.
[24] Eng, J. A., 2002, "Characterization of Pressure Waves in HCCI Combustion," SAE Technical Paper No. 2002-01-2859.
[25] Weiss, G., 1975, "Time-Reversibility of Linear Stochastic Processes," J. Appl. Probab., **12**(4), pp. 831–836.
[26] Finney, C. E. A., Green, J. B., Jr., and Daw, C. S., 1998, "Symbolic Time-Series Analysis of Engine Combustion Measurements," SAE Technical Paper No. 980624.
[27] Bengtsson, J., Strandh, P., Johansson, R., Tunestål, P., and Johansson, B., 2004, "Closed-Loop Combustion Control of Homogeneous Charge Compression Ignition (HCCI) Engine Dynamics," Int. J. Adapt. Control Signal Process., **18**(2), pp. 167–179.